Accepted Manuscript

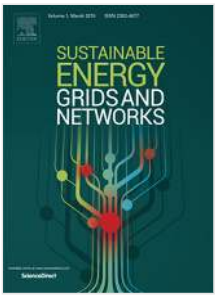

Stability and eigenanalysis of a sustainable remote area microgrid with a transforming structure

Farhad Shahnia

PII: S2352-4677(16)30087-X
DOI: http://dx.doi.org/10.1016/j.segan.2016.09.005
Reference: SEGAN 78

To appear in: *Sustainable Energy, Grids and Networks*

Received date: 22 April 2016
Revised date: 1 September 2016
Accepted date: 21 September 2016

Please cite this article as: F. Shahnia, Stability and eigenanalysis of a sustainable remote area microgrid with a transforming structure, *Sustainable Energy, Grids and Networks* (2016), http://dx.doi.org/10.1016/j.segan.2016.09.005

Stability and Eigenanalysis of a Sustainable Remote Area Microgrid with a Transforming Structure

Farhad Shahnia

School of Engineering and Information Technology, Murdoch University, Perth, Australia.

(Email: F.Shahnia@murdoch.edu.au, Phone: +61-8-93607429)

Abstract-Electrification of remote and rural areas is usually in the form of a standalone power system that operates self-sufficiently. Renewable energy resources, if available in such areas, are expected to have a large and ultimately, a full share of electricity generation in these areas to lessen the levelized cost of electricity for the operators. Thereby, the electric network of such remote areas can be considered as a sustainable microgrid (MG). Larger remote areas can be supplied by several MGs, each with a different operator (owner) and running independently. The occasional power deficiency and overloading of those MGs can be addressed by local support from the floating energy storages, or by importing power from a neighboring MG, after interconnecting the MGs temporarily. Thus, such MGs are expected to experience a transformation in their structure; a small change when new energy storage systems are connected and a significant alteration when it is coupled with another MG. Before such actions, the stability of the new system is vital to be cautiously examined to intercept the transformation, if instability is to occur. An eigenanalysis-based small signal stability evaluation technique is used in this research for an MG with a transforming structure. The analysis will be used as a decision-making process prior to a change in the MG. If the new system is defined to be unstable, the analysis can provide a range of control parameters for the energy resources to guarantee the stability of the new system. Through MATLAB-based analyses, the impact of the number and rating of the sources and loads, as well as the system topology of one MG on the stability of the system of coupled MGs, is evaluated. Moreover, the impacts of the number, energy capacity, rate of discharge and state of charge of the energy storage systems are assessed.

Index Terms-Coupled microgrids, Distributed energy resources, Battery storage systems, Overload management.

1. Introduction

Rural/remote towns around the world are usually supplied by stand-alone (community) power systems if the expansion of utility grid is not cost-effective due to significantly long distances and low demands) [1-3]. As an example, remote areas of Australia, covering 86% of the country and home to 3% of its population, are mostly supplied by stand-alone power systems [4]. Electrification of such areas is a challenge for utilities because of the area accessibility, economic factors, and the sustainability perspective [5-6]. The technical challenges in planning and operating remote area power systems is reviewed in [7]. As an alternate to grid-connected remote areas, the electricity is usually generated at such sites by diesel/gas-based generators; however, the fuel cost and its transportation difficulties increase the levelized cost of electricity [2, 8-9]. When a renewable resource is ample in those

areas (e.g. the solar energy availability in the Australian outback, and wind energy availability in its remote coastal areas), a larger portion of the electricity demand can be supplied from such resources [10-11]. Thereby, the need for diesel/gas-based generators can be minimized or removed, and all of the electricity demand in such areas can be supplied by renewable resources. In such a case, energy storage systems may also be required to store and return back the energy, in accordance with the intermittencies of the resources [12]. Thus, the electricity system of such remote areas can be considered as a sustainable microgrid (MG), composed of renewable energy-based, converter-interfaced distributed energy resources (DERs) and operating as an island [1-10]. Enough generation capacity should be available in the DERs to meet the demand as there is no backup support from a utility grid [13-15]. Large remote towns can be supplied by several independent MGs, where each may have a different owner (operator) and each is responsible for supplying loads of a specific region [2]. Therefore, the distribution network of a large remote town can resemble the system of Fig. 1.

Intermittency of non-dispatchable (e.g. solar and wind-based) DERs in addition to load uncertainties can cause an imbalance between power generation and demand in an MG at some intervals [16-17]. Any deficiency in the generation capability versus the demand (referred to as MG overloading in the rest of this paper) results in voltage or frequency drop. The easiest solution for grid-connected MGs in such circumstances is importing power from the utility grid; however, such an option is not available for remote area MGs. Thereby, the solutions that can be considered are employment of dispatchable DERs (e.g. diesel generators) [18], expansion of the utility grid to the MG site and their interconnection [13], under-frequency/voltage load-shedding [19], utilization of floating battery energy storage (BES) systems [20], and coupling of the overloaded MG to one/more neighboring MG(s) [21].

Assuming the possibility of coupling the neighboring MGs, each overloaded MG in the system of Fig. 1 may be supported by other MGs. Based on this idea, a transformative architecture is proposed in [22] for coupling the MGs to improve the system self-healing in the case of faults. Power trading among MGs in the system of coupled MGs (CMG) is addressed in [23]. Optimal control of a distribution network composed of utility-connected MGs that form a CMG is studied in [24] while an interactive control of CMGs is presented in [25] to guarantee effective load sharing. Dynamic operation of DERs within CMGs is investigated in [26], and the dynamic security of the CMGs is examined in [27]. The interaction among the DERs of the MGs in a CMG system is also investigated in [28]. Coupling of MGs can be realized by back-to-back converters or normally-open interconnecting static switches (ISSes) [29-30].

Coupling an overloaded MG to a neighboring MG is a successful strategy to delay or eliminate the necessity of load-shedding [30]. A decision-making-based approach is proposed in [31] to determine the most suitable MG(s) to be coupled with the overloaded MG, which considers the available surplus power, electricity cost, reliability, supply security, and the distance among MGs, as well as the maximum voltage/frequency deviation in the CMG. In [30], the proper conditions and constraints for forming a CMG between the overloaded MG and the selected suitable neighboring MG are developed, which are based on monitoring the frequency and apparent power of the overloaded and the neighboring MG. This research is further extended in [32] to consider an additional level of support

by floating BES systems, based on which, at the first level of overloading detection, the BES system of the overloaded MG connects to provide support to the MG. If the level of support is not enough or if the stored energy of the BES system drains over time, external support is facilitated by forming a CMG. Under such a scenario, if the CMG system is overloaded, the BES system of the neighboring MG will also connect to support the CMG system. By the help of the developed criteria in [30, 32], all or a portion of the demand of an MG is supported by the local BES system or is imported from the neighboring MG, leading to a reduced/minimized necessity and rate of load-shedding.

Before connecting a BES system or forming a CMG, the stability of the new system should be carefully analyzed to accept or reject the change. Alternatively, if instability is observed, a range of droop control coefficients should be defined for the DERs to enable the connection of the BES system or interconnection of MGs. Thus, the small signal stability (SSS) analysis is required before each change to prevent the changes that can lead to instability. Fig. 2 illustrates schematically the flowchart of the overload management technique of [30, 32] in which the main research focus of this paper is also highlighted.

The SSS of a multi-synchronous machine-based system is extended to MGs in literature, and eigenanalysis, frequency-response (impedance-based) methods, as well as a micro-based approach have been used for this purpose [34-35]. A review of different SSS analysis techniques including transformation into a rotating direct-quadratic reference frame, dynamic phasors, reduced-order modeling, and harmonic linearization is presented in [36]. Reference [33] has carried out a review of different SSS analyses for an MG in grid-connected and islanded modes. In eigenanalysis, the system is represented by a set of state-space equations and the eigenvalues of the system are calculated from the state matrix of the system [37]. This analysis predicts the response of an MG when the system parameters are changed. An eigenanalysis-based SSS model of an MG composed of converter-interfaced DERs is presented in [34, 37-45]. These studies have focused on an MG with a known structure which has a constant number of DERs and loads and have not considered any changes in the structure of the MG, neither on the number of DERs and loads. In other words, the stability of an MG with a transforming structure has not been investigated in details. This is the research gap that is focused in this paper and has to be addressed to analyze the stability of a transforming MG that is proposed for overload management in remote areas.

Investigating the stability of an MG with a transforming structure may seem straightforward at the first thought; however, this paper shows that its changes are irregular when the MG is coupled with another MG (or a BES system is added to it), depending on the conditions of the newly created system. To this end, this research tries to evaluate how the stability is affected when

- the number of DERs increases in the MG, assuming that the total power generation is increased/constant,
- the number of loads increases in the MG, assuming that the total power demand is increased/constant,
- BES systems are added to the MG,
- the state of charge (SoC) of a BES system is reduced over time,
- multiple BES systems, each with a dissimilar SoC, are present,

- considering different length and X/R ratio of the lines, and
- it couples with a different MG which has a radial/loop topology.

2. Network under Consideration

Consider the remote area network of Fig. 1, composed of three MGs. The MGs are thought to be interconnected together through a normally open ISS and tie-lines. Normally, each MG operates in islanded mode and independently from the other MGs. N_{DER} converter-interfaced DERs, N_{BES} BES systems, N_{load} loads, N_{line} lines and N_{bus} buses are assumed in each MG. Note that in this research, a BES system is not categorized under a DER although both of them are assumed to be converter-interfaced. Operation of DERs and BES systems are discussed below:

2.1. Operation of DERs in the MG

A review of different control methods for the DERs of an MG is presented in [46]. In this research, it is thought that the voltage magnitude and frequency at the converter output of DER-i, $i \in \{1, \ldots, N_{DER}\}$ is regulated by conventional frequency droop control, described as [30]

$$\begin{aligned} f_{\text{DER-}i} &= f^{\max} - m_{\text{DER-}i} P_{\text{DER-}i} \\ \left|V_c\right|_{\text{DER-}i} &= V^{\max} - n_{\text{DER-}i} Q_{\text{DER-}i} \end{aligned} \tag{1}$$

where m is the P-f droop coefficient in Hz/W, n is the Q-V droop coefficient in V/Var, V^{max} and f^{max} are respectively the maximum allowed voltage magnitude and frequency, and P and Q are respectively the average active and reactive powers injected by the DER to its terminal. The subscript $_{DER}$ represents the DERs. Note that (1) is valid when the active and reactive powers are decoupled by high X/R ratio of the lines. Alternatively, the generalized droop control should be used [47]. It is noteworthy that if the cost of electricity generation by different DERs is unalike, the MG owners may adopt a cost-prioritized droop technique, such as the one presented in [48].

When a DER increases its output active and reactive power from zero to the maximum level, the DER frequency and voltage magnitude reduces respectively from f^{max} to f^{min} and from V^{max} to V^{min} where ^{max} and ^{min} respectively show the maximum and minimum allowable limits. Thereby, m and n are derived for DER-i from [26]

$$\begin{aligned} m_{\text{DER-}i} &= (f^{\max} - f^{\min}) / P^{\text{cap}}_{\text{DER-}i} \\ n_{\text{DER-}i} &= (V^{\max} - V^{\min}) / 2Q^{\text{cap}}_{\text{DER-}i} \end{aligned} \tag{2}$$

where ^{cap} illustrates the capacities of the DERs. In this research, it is assumed that f^{max}, f^{min}, V^{max} and V^{min} of both MGs are the same. Thus, the DERs of both MGs will have the same $\Delta f = f^{max} - f^{min}$ and the same $\Delta V = V^{max} - V^{min}$ values, albeit their different capacities.

The ratio of the active and reactive powers generated by any two DERs in an MG (e.g. DER-i and DER-j) is desired to be equal to the ratio of their nominal powers (capacities) and is controlled by the reciprocal of the ratio of their droop coefficients [26]; i.e.,

$$\begin{aligned} P_{\text{DER-}j} / P_{\text{DER-}i} &\approx P^{\text{cap}}_{\text{DER-}j} / P^{\text{cap}}_{\text{DER-}i} = m_{\text{DER-}i} / m_{\text{DER-}j} \\ Q_{\text{DER-}j} / Q_{\text{DER-}i} &\approx Q^{\text{cap}}_{\text{DER-}j} / Q^{\text{cap}}_{\text{DER-}i} = n_{\text{DER-}i} / n_{\text{DER-}j} \end{aligned} \tag{3}$$

Note that a DER in this research refers to a combination of energy resource with its smoothing energy storage sys-

tem and energy management system; thereby, all DERs are thought to be dispatchable. In addition, they are assumed capable of generating the powers defined by (3). If due to environmental reasons, the output power of a DER is saturated below the desired value of (3), the other DERs will share the rest of the load based on the ratios given in (3).

2.2. Operation of BES Systems in the MG

Every BES system has a nominal capacity, explained in kWh or Ah. However, as it injects active power to the MG, its stored energy is reduced. As a result, a BES is characterized based on its stored energy or SoC, rather than its nominal capacity. Thereby, a new operation mechanism is proposed in [49] for the floating BES systems in an MG, compared to the DERs. This approach guarantees that BES systems in an MG, each with a dissimilar nominal capacity and SoC, will operate such that the SoCs of all BES systems reduce to the minimum acceptable SoC (SoC^{min}) at the same time, regardless of their capacity and initial charge. It is to be highlighted that this is the desired condition in an MG unless the BES systems have different owners in which they compete to discharge based on a dynamic electricity tariff. To achieve this preferred result, it is desired for a BES system with lower SoC to inject less active power compared to a BES system with a higher SoC. This is regardless of the nominal capacities of the BES systems. To realize this, the rate of discharge (RoD) of BES-*i*, ($RoD_{\text{BES-}i}$), $i \in \{1, \ldots, N_{\text{BES}}\}$ is defined as

$$RoD_{\text{BES-}i} = SoC^{\text{d}}_{\text{BES-}i} P^{\text{cap}}_{\text{BES-}i} \tag{4}$$

where

$$SoC^{\text{d}}_{\text{BES-}i} = \begin{cases} 1 & SoC = 1 \\ 0.9 & 0.9 \le SoC < 1 \\ \vdots & \\ 0.2 & 0.2 \le SoC < 0.3 \end{cases}$$

and $_{\text{BES}}$ represents BES systems. From (4), the *P-f* droop coefficient of BES-*i* ($m_{\text{BES-}i}$) can be defined as

$$m_{\text{BES-}i} = \Delta f / RoD_{\text{BES-}i} \tag{5}$$

Note that m_{BES} varies discretely and not continuously as it uses SoC^{d} instead of continuously varying SoC.

From (4) and (5), it can be seen that the output active power by BES-*i* reduces as SoC^{d} becomes smaller. Thereby, a smaller portion of the capacity of the converter of the BES ($S^{\text{cap}}_{\text{BES}}$) is utilized for active power flow. The unused portion of the converter capacity can then be used for reactive power exchange. Therefore, in this research, it is assumed that in addition to active power exchange between the BES system and the MG, a reactive power exchange also occurs. The available capacity for reactive power in the converter of BES-*i* ($Q^{\text{av}}_{\text{BES-}i}$) is defined dynamically as [50]

$$Q^{\text{av}}_{\text{BES-}i} = \sqrt{\left(S^{\text{cap}}_{\text{BES-}i}\right)^2 - \left(RoD_{\text{BES-}i}\right)^2} \tag{6}$$

and is used to defined the *V-Q* droop coefficient of BES-*i* ($n_{\text{BES-}i}$) as

$$n_{\text{BES-}i} = \Delta V / 2Q^{\text{av}}_{\text{BES-}i} \tag{7}$$

As a result, the ratio of the active and reactive powers between a DER and a BES system in the MG (e.g. DER-*i* and BES-*i*) is as

$$\begin{aligned} P_{\text{BES-}i}/P_{\text{DER-}i} &\approx RoD_{\text{BES-}i}/P^{\text{cap}}_{\text{DER-}i} = m_{\text{DER-}i}/m_{\text{BES-}i} \\ Q_{\text{BES-}i}/Q_{\text{DER-}i} &\approx Q^{\text{av}}_{\text{BES-}i}/Q^{\text{cap}}_{\text{DER-}i} = n_{\text{DER-}i}/n_{\text{BES-}i} \end{aligned} \tag{8}$$

Note that the reactive power exchange between the converter of the BES system and the MG does not affect the stored energy and the SoC of the BES system.

3. Eigenanalysis-Based Small Signal Stability Evaluation

The DERs in this research are thought to be connected to the MG through a voltage source converter (VSC), which is composed of three parallel H-bridges. The structure and closed-loop control of the VSCs are presented in [30, 32] and are not discussed here. An LCL filter (i.e. L_{f} , C_{f}, and L_{T}) is used at the VSC output. A voltage control technique is utilized in *abc* frame to track the desired voltage at the output of the VSC (i.e., across the capacitors C_{f}). The linearized state-space description of DER-*i*, with such a VSC and filter structure and its closed-loop control, can be represented in direct-quadrant frame around its equilibrium point as [37, 41-43]

$$\Delta\dot{\mathbf{x}}^{i}_{\text{DER}} = \mathbf{A}^{i}_{\text{DER}}\,\Delta\mathbf{x}^{i}_{\text{DER}} + \mathbf{B}^{i}_{\text{DER}}(\Delta\mathbf{Z}^{i}_{\text{DER}})^{\text{ref}} + \mathbf{C}^{i}_{\text{DER}}\Delta\mathbf{v}^{i}_{\text{DER}} \tag{9}$$

where $\mathbf{x}_{\text{DER}} = [i_1^{\text{d}} \;\; i_1^{\text{q}} \;\; i_2^{\text{d}} \;\; i_2^{\text{q}} \;\; v_{\text{c}}^{\text{d}} \;\; v_{\text{c}}^{\text{q}}]^T$ and $\mathbf{Z}_{\text{DER}} = [i_2^{\text{d}} \;\; i_2^{\text{q}} \;\; i_{\text{c}}^{\text{d}} \;\; i_{\text{c}}^{\text{q}} \;\; v_{\text{c}}^{\text{d}} \;\; v_{\text{c}}^{\text{q}}]^T$ while i_1 and i_2 are respectively the current of L_{f} and L_{T}, i_{c} and v_{c} are respectively the current and voltage of C_{f}, **A** and **B** are system matrices; **v** is the terminal voltage, and T is the transpose operator. Since it is assumed that the BES systems have the same VSC and filter structure and closed-loop control system to those of the DERs, in a similar fashion to (9), the linearized state-space equations for BES-*i* system around its equilibrium point can be represented as

$$\Delta\dot{\mathbf{x}}^{i}_{\text{BES}} = \mathbf{A}^{i}_{\text{BES}}\,\Delta\mathbf{x}^{i}_{\text{BES}} + \mathbf{B}^{i}_{\text{BES}}(\Delta\mathbf{Z}^{i}_{\text{BES}})^{\text{ref}} + \mathbf{C}^{i}_{\text{BES}}\Delta\mathbf{v}^{i}_{\text{BES}} \tag{10}$$

The loads in this study are thought as constant impedance RL loads. Therefore, the linearized state-space equation of load-*j* connected to bus-*jj* in the MG can be represented around its equilibrium point as [37, 41-43]

$$\Delta\dot{\mathbf{x}}^{j}_{\text{load}} = \mathbf{A}^{j}_{\text{load}}\,\Delta\mathbf{x}^{j}_{\text{load}} + \mathbf{C}^{j}_{\text{load}}\Delta\mathbf{v}^{jj}_{\text{load}} \tag{11}$$

where $\mathbf{x}_{\text{load}} = [i^{\text{d}}_{\text{load}} \;\; i^{\text{q}}_{\text{load}}]^T$. Likewise, the lines in this study are assumed to be as constant RL branches; thereby, the linearized state-space equation of line-*k* between adjacent buses *kk* and *ll* in the MG can be represented around its equilibrium point as [37, 41-43]

$$\Delta\dot{\mathbf{x}}^{k}_{\text{line}} = \mathbf{A}^{k}_{\text{line}}\,\Delta\mathbf{x}^{k}_{\text{line}} + \mathbf{C}^{k}_{\text{line}}\,\Delta\mathbf{v}_{\text{MG}} \tag{12}$$

where $\mathbf{x}_{\text{line}} = [i^{\text{d}}_{\text{line}} \;\; i^{\text{q}}_{\text{line}}]^T$.

Combining the state-space descriptions of all DERs, BES systems, loads and lines in the MG along with their output average active/reactive powers (**p**, **q**), angles of voltages (**δ**) and SoC of BES systems (**SoC**), the homogeneous form of the MG ($\mathbf{A}^{\text{H}}_{\text{MG}}$) is described as

$$\Delta\dot{\mathbf{x}}_{\text{MG}} = \mathbf{A}^{\text{H}}_{\text{MG}}\,\Delta\mathbf{x}_{\text{MG}} \tag{13}$$

where

$$\mathbf{x}_{\mathrm{MG}}=\left[\begin{array}{c}\overbrace{\mathbf{x}_{\mathrm{DER}}^{1}\cdots\mathbf{x}_{\mathrm{DER}}^{N_{\mathrm{DER}}}}^{\text{DERs}}\ \overbrace{\mathbf{x}_{\mathrm{BES}}^{1}\cdots\mathbf{x}_{\mathrm{BES}}^{N_{\mathrm{BES}}}}^{\text{BES Systems}}\ \overbrace{\mathbf{x}_{\mathrm{load}}^{1}\cdots\mathbf{x}_{\mathrm{load}}^{N_{\mathrm{load}}}}^{\text{Loads}}\ \overbrace{\mathbf{x}_{\mathrm{line}}^{1}\cdots\mathbf{x}_{\mathrm{line}}^{N_{\mathrm{line}}}}^{\text{Lines}}\\ \overbrace{\mathbf{p}_{\mathrm{DER}}^{1}\cdots\mathbf{p}_{\mathrm{DER}}^{N_{\mathrm{DER}}}}^{\text{DERs}}\ \overbrace{\mathbf{p}_{\mathrm{BES}}^{1}\cdots\mathbf{p}_{\mathrm{BES}}^{N_{\mathrm{BES}}}}^{\text{BES Systems}}\ \overbrace{\mathbf{q}_{\mathrm{DER}}^{1}\cdots\mathbf{q}_{\mathrm{DER}}^{N_{\mathrm{DER}}}}^{\text{DERs}}\ \overbrace{\mathbf{q}_{\mathrm{BES}}^{1}\cdots\mathbf{q}_{\mathrm{BES}}^{N_{\mathrm{BES}}}}^{\text{BES Systems}}\\ \overbrace{\boldsymbol{\delta}_{\mathrm{DER}}^{1}\cdots\boldsymbol{\delta}_{\mathrm{DER}}^{N_{\mathrm{DER}}}}^{\text{DERs}}\ \overbrace{\boldsymbol{\delta}_{\mathrm{BES}}^{1}\cdots\boldsymbol{\delta}_{\mathrm{BES}}^{N_{\mathrm{BES}}}}^{\text{BES Systems}}\ \overbrace{\mathbf{SoC}_{\mathrm{BES}}^{1}\cdots\mathbf{SoC}_{\mathrm{BES}}^{N_{\mathrm{BES}}}}^{\text{BES Systems}}\end{array}\right]^{T}$$

From (13), the eigenvalues of the MG (λ_{MG}) are defined as the roots of

$$\det(\lambda_{\mathrm{MG}}\mathbf{I}-\mathbf{A}_{\mathrm{MG}}^{\mathrm{H}})=0 \tag{14}$$

where $\mathbf{I}$ is the identity matrix with the same size of $\mathbf{A}_{\mathrm{MG}}^{\mathrm{H}}$ and det(.) is the determinant function. Considering the fact that each DER has 9 states (i.e., 4 states of current, two states of voltage, two states of power and one state of angle), each BES system has 10 states (i.e., the same states mentioned for the DERs as well as the SoC state), each load and line have two states of current, the number of the eigenvalues for an MG system ($N_{\lambda}^{\mathrm{MG}}$) is given by

$$N_{\lambda}^{\mathrm{MG}}=9N_{\mathrm{DER}}+10N_{\mathrm{BES}}+2N_{\mathrm{load}}+2N_{\mathrm{line}} \tag{15}$$

For a CMG system consisting of N_{MG} MGs (where $N_{\mathrm{MG}} \geq 2$) that are interconnected through $N_{\text{Tie-line}}$ tie-lines, the linearized state-space equation can be expressed in the homogenous form of

$$\Delta\dot{\mathbf{x}}_{\mathrm{CMG}}=\mathbf{A}_{\mathrm{CMG}}^{\mathrm{H}}\,\Delta\mathbf{x}_{\mathrm{CMG}} \tag{16}$$

where $\mathbf{x}_{\mathrm{CMG}}=\left[\overbrace{\mathbf{x}_{\text{MG-1}}\cdots\mathbf{x}_{\text{MG-}N_{\mathrm{MG}}}}^{\text{MGs}}\ \overbrace{\mathbf{x}_{\text{Tie-line-1}}\cdots\mathbf{x}_{\text{Tie-line-}N_{\text{Tie-line}}}}^{\text{Tie-lines}}\right]^{T}$.

Similar to (14), the eigenvalues of the CMG (λ_{CMG}) are the roots of [51]

$$\det(\lambda_{\mathrm{CMG}}\mathbf{I}-\mathbf{A}_{\mathrm{CMG}}^{\mathrm{H}})=0 \tag{17}$$

where $\mathbf{I}$ has the same size of $\mathbf{A}_{\mathrm{CMG}}^{\mathrm{H}}$. Thereby, the number of the eigenvalues for a CMG system ($N_{\lambda}^{\mathrm{CMG}}$) is given by

$$N_{\lambda}^{\mathrm{CMG}}=N_{\lambda}^{\text{MG-1}}+N_{\lambda}^{\text{MG-2}}+\ldots+N_{\lambda}^{\text{MG-}N_{\mathrm{MG}}}+2N_{\text{Tie-line}} \tag{18}$$

For a stable MG or CMG system, all eigenvalues must be on the left side of the imaginary axis of *s*-plane, i.e., Re(λ) = σ < 0, where $\lambda = \sigma + j\upsilon$ and Re(.) represents the real function [51]. The eigenvalues located very far from the imaginary axis of the *s*-plane (σ << 0) usually damp very quickly. These eigenvalues have a smaller impact on the stability of the system and thus are not discussed in this paper. The closer eigenvalues to the imaginary axis are the dominant eigenvalues of the system, and the MG or CMG system becomes unstable if any of them is relocated to the right side of the imaginary axis.

After defining the eigenvalues of the system, an analysis can be carried out to investigate the impact of different states on the system performance. Each eigenvalue of the system is affected by a group of its states. The contribu-

tion of each of the states of $\mathbf{x}_{MG}$ or $\mathbf{x}_{CMG}$ on each of the eigenvalues can be calculated from the participation factor matrix (**PF**), defined as [51-52]

$$\mathbf{PF} = (\mathbf{\Gamma}^{-1})^{T} \otimes \mathbf{\Gamma} \tag{19}$$

where $\mathbf{\Gamma}$ is the right eigenvectors matrix of $\mathbf{A}_{CMG}^{H}$ and $\otimes$ indicates the element by element production. In (19), $\mathbf{PF}(x,y)$ represents the contribution of state x on eigenvalue y. The states that have the highest impact (i.e., the largest contribution) on an eigenvalue are referred to as the effective states of that eigenvalue in the rest of this paper. The normalized weighting of each state on each eigenvalue is calculated from [51-52]

$$\left\|\mathbf{PF}(x,y)\right\| = \left|\mathbf{PF}(x,y)\right| / \sum_{\mu}\left|\mathbf{PF}(\mu,y)\right| \tag{20}$$

where μ shows all states of eigenvalue y.

SSS analysis can determine the range of the droop coefficients in which each MG or the CMG system is marginally stable [53]. To this end, using a sensitivity analysis, droop coefficient m is normally varied between $0.1m_o$ and $10m_o$ around the operating point of m_o. Likewise, droop coefficient n is also varied. Let us denote the very first m and n in which a stable system becomes critically (marginally) stable as $m_{critical}$ and $n_{critical}$, respectively. If all DERs have the same nominal powers, $m_{critical}$ and $n_{critical}$ are valid for all DERs. However, if they have different nominal powers, their $m_{critical}$ and $n_{critical}$ have a ratio as given by (3). This is also valid for the BES systems. Thus, $m_{critical}$ corresponds to a specific P_{DER}^{cap} while $n_{critical}$ corresponds to a specific Q_{DER}^{cap}. Thereby, in this paper where the capacities and numbers of the DERs, as well as the SoC, RoD, and energy capacity of the BES systems, are varied, instead of $m_{critical}$ and $n_{critical}$, two other stability margins are defined, namely $\Delta f_{critical}$ and $\Delta V_{critical}$. These two quantities are derived from (2) and are expressed as

$$\begin{aligned} \Delta f_{critical}\,\% &= \left(m_{critical\text{-}i} \times P_{DER\text{-}i}^{cap}\right) / f_{nominal} \times 100 \\ \Delta V_{critical}\,\% &= \left(n_{critical\text{-}i} \times 2Q_{DER\text{-}i}^{cap}\right) / V_{nominal} \times 100 \end{aligned} \tag{21}$$

which can be calculated from any of the DERs.

4. Numerical Analysis Results

As discussed in the Introduction Section, the SSS analysis of the MG needs to be evaluated prior to the interconnection of the MG to another MG or prior to the connection of a BES system. In this Section, first, the stability of two individual MGs is evaluated by the help of the eigenanalysis, realized in MATLAB®. Later, the stability of the CMG, composed of them, is evaluated. The study is further enhanced by investigating the impact of different variables if one of the MGs on the stability of the CMG. In the end, the stability of an MG or CMG system with BES systems is evaluated.

4.1. Stability of Independent MGs

Let us consider MG-1 and MG-2 of Fig. 1, with a detailed structure shown in Fig. 3. MG-1 is assumed to have two converter-interfaced DERs (connected to its bus-1 and 2) and one load (connected to its bus-3) in a loop configuration. MG-2 is thought to have 4 converter-interfaced DERs (connected to its bus-1 to 4) and one load (connected to

its bus-5) in a loop configuration. It is assumed that bus-4 of MG-1 can interconnect to bus-6 of MG-2 through a tie-line and an ISS. For simplicity, it is thought that all DERs have the same nominal power and thus, the same droop coefficients m and n. In addition, it is assumed that the distances of the buses from each other and the cross-section of the conductors between them are the same; hence, the impedances of all lines are also equal. This system is referred to as the base case for MG-1 and MG-2 in the rest of this paper. The technical data of the network are provided in Table A1 in the Appendix. The stability of each MG when operating independently is evaluated below:

4.1.1. Stability Studies of MG-1

Let us assume that the operating point droop coefficients for this system are m_o = 0.333 Hz/kW and n_o = 2.3 V/kVAr. To evaluate the system stability, the droop coefficients are varied in the range of $0.0333 \le m \le 3.333$ and $0.23 \le n \le 23$. Fig. 4a illustrates the eigenvalue trajectory of this system when m is varied. From this figure, it can be seen that the stable system becomes unstable for $m_{critical}$ = 3.1684 Hz/kW (i.e., $\Delta f_{critical}$ = 19.010%). This figure only shows the dominant eigenvalues of the system, and the eigenvalues of the system at the operating point are shown by asterisk □. This trajectory is composed of two complex conjugate critical eigenvalues (λ_1 and λ_2) and some non-critical eigenvalues.

Fig. 4b illustrates the dominant eigenvalue trajectory of this system when n is varied. The operating point eigenvalues are again shown by asterisk □. From this figure, it can be seen that the system becomes unstable for $n_{critical}$ = 3.3662 V/kVAr (i.e., $\Delta V_{critical}$ = 7.317%). This trajectory is also composed of two complex conjugate critical eigenvalues and some non-critical eigenvalues. The characteristics of each of these eigenvalues including their real part (σ), imaginary part (υ), damping ratio (ζ), undamped natural frequency (ω_n), oscillation period (T), and number of cycles to damp by 50% ($NoC_{50\%}$) are provided in Table 1. The pie chart of Fig. 4c illustrates the participation factor of different states of the system on the critical eigenvalues. From this figure, it can be seen that λ_1 and λ_2 are significantly affected by the output current states of both DERs (i.e., $(i_2^d)_{DER\text{-}1}$, $(i_2^q)_{DER\text{-}1}$, $(i_2^d)_{DER\text{-}2}$, and $(i_2^q)_{DER\text{-}2}$, each with a weighting of 23.86%) while the rest of the system states altogether have an impact of 4.60%.

To assess the impact of the nominal powers of the DERs on the SSS of MG-1, an analysis is carried out in which the nominal power of both DERs is increased from 40 to 200% of the nominal power of the base case. Fig. 4d illustrates $\Delta f_{critical}$ and $\Delta V_{critical}$ for MG-1 in these scenarios. From these figures, it can be seen that $\Delta f_{critical}$ increases from 3.691% (for 40% of the nominal power) to 19.010% (for 100% of the nominal power). In addition, it can be seen that $\Delta V_{critical}$ increases from 2.805% (for 40% of the nominal power) to 14.822% (for 200% of the nominal power of the base case). No instability is observed when the nominal power of the DERs is increased above 100% of the nominal power for the variations of m, in the above-mentioned ranges.

A different analysis is conducted to consider the impact of the ratio of the nominal power of the DERs, in which the ratio of the nominal power of DER-2 versus the nominal power of DER-1 is varied from 1 to 9, while the total power generation capacity of the DERs is kept constant and equal to that of the base case. Fig. 4e illustrates $\Delta f_{critical}$ and $\Delta V_{critical}$ for MG-1 in these scenarios. From this figure, it can be seen that $\Delta f_{critical}$ decreases from 19.010% (for

$P_{DER\text{-}2}$ / $P_{DER\text{-}1}$ = 1) to 2.338% (for $P_{DER\text{-}2}$ / $P_{DER\text{-}1}$ = 8). MG-1 is found to be unstable if $P_{DER\text{-}2}$ / $P_{DER\text{-}1}$ becomes larger than 8. It can also be seen that $\Delta V_{critical}$ decreases from 7.317% (for $P_{DER\text{-}2}/P_{DER\text{-}1}$=1) to 1.922% (for $P_{DER\text{-}2}/P_{DER\text{-}1}$=9).

4.1.2. Stability Studies of MG-2

Let us assume the same operating point droop coefficients of MG-1 for MG-2. The SSS of this system is also analyzed by a similar sensitivity analysis in which *m* and *n* are varied in the above-mentioned ranges. The dominant eigenvalue trajectories of MG-2 are shown in Fig. 5a-b. From these figures, it can be seen that the system is stable for $m_{critical}$ = 3.0193 Hz/kW (i.e., $\Delta f_{critical}$ = 18.115%) and $n_{critical}$ = 3.118 V/kVAr (i.e., $\Delta V_{critical}$ = 6.778%). This system has 8 complex conjugate critical eigenvalues (λ_1-λ_8) and some non-critical eigenvalues for *m* variation while it has 6 complex conjugate critical eigenvalues and some non-critical eigenvalues for *n* variation. Table 1 also describes the characteristics of the eigenvalues of MG-2. Due to the resemblance of the considered DER structure and control, as well as the load and line types in MG-1 and 2, there is a similarity in some of the eigenvalues of these MGs and their characteristics, as seen from this table. From the pie charts of Fig. 5c, it can be seen that the critical eigenvalues of MG-2 are either affected by the output current states of the DERs (i.e., λ_1-λ_6), or by the current states of the lines (i.e., λ_7-λ_8). It is to be noted that λ_7 and λ_8 have a real part of –314.159 at the system operating point (based on the data of Table 1), which is beyond the real axis range of Fig. 5a. However, for larger *m* variations, they relocate to a closer distance from the imaginary axis (falling within the real axis range of the figure). By a further increase in *m*, they cause instability for MG-2.

4.2. Stability of a CMG System

Now let us assume that it is desired to couple MG-1 to MG-2 by closing the ISS between them (see Fig. 5). Both MGs have a loop structure, both have the same load demand, and the only dissimilarity is that MG-1 has 2 DERs while MG-2 has 4 DERs. The tie-line is also assumed to have the same impedance of the lines of the MGs. This system is referred to as the CMG base case in the rest of this paper.

To define the eigenvalue trajectories for the CMG, at the beginning, the new operating points for all state variables of the CMG are defined for the instant that the MGs are connected, and the system is in the steady-state condition. Then, the sensitivity analysis is applied to the linearized description of the newly created system and around its defined equilibrium points. Fig. 6a-b illustrates the dominant eigenvalue trajectories for the CMG base case. From this figure, it can be seen that the CMG is stable for $m_{critical}$ = 3.0011 Hz/kW (i.e., $\Delta f_{critical}$ = 18.006%) and $n_{critical}$ = 3.0729 V/kVAr (i.e., $\Delta V_{critical}$ = 6.680%). Thus, it can be seen that the system will lower stability margin (i.e., MG-2) forces the stability margin of the other MG to be reduced. The characteristics of the dominant eigenvalues of the CMG system are also provided in Table 1. As the CMG is composed of MG-1 and MG-2, there is a similarity between the eigenvalues of CMG with those of MG-1 and MG-2, as seen from this table. The participation factor of each state of the CMG on its dominant eigenvalues is shown in the pie charts of Fig. 6c. From this figure, it can be seen that the dominant eigenvalues of the CMG system are affected either by the output current states of the DERs of both MGs (shown in Fig. 6c(**i**)-(**iv**)), or by the current states of the MG lines and the tie-line (shown in Fig. 4c(**v**)),

or by the angle and output average active power states of the DERs of both MGs (shown in Fig. 6c(**vi**)). In this system, λ_9 and λ_{10} have the same behavior as λ_7 and λ_8 of MG-2.

A comparison between the operating point eigenvalues (λ^{op}) of MG-1, MG-2 and those of the CMG is presented in Fig. 6d. In this figure, asterisk ☆ illustrates the eigenvalues which are significantly influenced by the output current states of the DERs while asterisk ○ illustrates the ones that are significantly influenced by the output average active power and angle states. The rest of the eigenvalues are shown by asterisk ✳. From this figure, it can be seen that the loci of λ^{op}_{CMG} affected by a specific group of states are in the same loci of $\lambda^{op}_{MG\text{-}1}$ and $\lambda^{op}_{MG\text{-}2}$ that are affected by the similar states.

Now it is desired to define a trend for $\Delta f_{critical}$ and $\Delta V_{critical}$ of the CMG if some of the parameters of MG-2 are varied while the parameters of MG-1 are constant. The analysis will be focused on varying the number and nominal power of the DERs, number, and demand of loads, length and X/R ratio of lines as well as the system topology (loop/radial) in MG-2. For the analyses in which the number of loads/DERs is increased, MG-2 is assumed to have a larger number of buses (to which the loads/DERs are connected) and lines (that interconnect the new buses). However, the impedances of all new lines are thought to be the same as those of MG-2 base case. In addition, the new system is assumed to have a loop configuration.

4.2.1. Impact of DERs

First, a study is conducted to analyze the SSS of the CMG system with respect to the number and nominal powers of the DERs. For this, let us assume that the number of the DERs of MG-2 is increased sequentially from 4 to 12 while all DERs are thought to have the same nominal power of those in MG-2 base case. To this end, each DER is thought to be connected to a separate bus which is interconnected to the other adjacent DER buses with the same line impedances of the rest of the system. This assumption represents an MG with multiple DERs, each with plug and play characteristic (that can be on or off at different intervals). For each case, the new steady-state operating points of the system are defined, and the system is linearized around its defined equilibrium points. Then, the eigenvalue trajectory is plotted for each case using a sensitivity analysis in which m is varied around the operating point of m_o, based on which the corresponding $m_{critical}$ is defined. Fig. 7a illustrates the evolution of eigenvalue trajectory for each case separately, as well as their $m_{critical}$. Using $m_{critical}$ of each case in (21), $\Delta f_{critical}$ is defined for the CMG in each case, and reported in Fig. 8a(i). In a similar way, the sensitivity analysis for n yields $\Delta V_{critical}$ for each case, as reported in Fig. 8a(ii). The first data in both of these subfigures correspond to the CMG base case. From these figures, it can be seen that $\Delta f_{critical}$ reduces slightly from 18.006% (for a CMG with 6 DERs) to 17.373% (for a CMG with 14 DERs). Similarly, $\Delta V_{critical}$ reduces slightly from 6.680 to 6.557%.

Another study is carried out to investigate the impact of the increase in the number of the DERs of MG-2 in the CMG if their total power generation capacity is kept constant and equal to that of MG-2 base case. Similar to the previous study, Fig. 7b illustrates the evolution of eigenvalue trajectory for each case, as well as the corresponding $m_{critical}$ for m variation, based on which $\Delta f_{critical}$ for the CMG in these scenarios is reported in Fig. 8b(i). Likewise,

$\Delta V_{critical}$ is calculated for the CMG in these scenarios after a sensitivity analysis on n, and reported in Fig. 8b(ii). The first data in both subfigures of Fig. 8b correspond to the CMG base case. From this figure, it can be seen that $\Delta f_{critical}$ reduces from 18.006% (for a CMG with 6 DERs) to 1.836% (for a CMG with 12 DERs) if the total power generation capacity in all scenarios are equal. The CMG is found to be unstable if MG-2 has 11 DERs or more. For this study, $\Delta V_{critical}$ decreases from 6.680% (for a CMG with 6 DERs) to 2.609% (for a CMG with 14 DERs).

The above analyses show that an increase in the number of the DERs of one of the MGs does not affect the stability margins of the CMG strongly if the generation capacity of the CMG increases; however, they are strongly affected if the generation capacity of the CMG is constant.

4.2.2. Impact of Loads

First, a study is carried out to evaluate the impact of the number of loads in the CMG system. For this, let us assume that the number of loads of MG-2 is increased sequentially from 1 to 9 while each load is assumed to have the same demand as that in MG-2 base case. To this end, each load is thought to be connected to a separate bus, which is interconnected to the other adjacent load buses with the same line impedances of the rest of the system. This assumption represents an MG with multiple loads, each with plug and play characteristic that turn on and off at different intervals. Fig. 9a illustrates $\Delta f_{critical}$ and $\Delta V_{critical}$ for the CMG in these scenarios where the first data in its both subfigures correspond to the CMG base case. From these figures, it can be seen that $\Delta f_{critical}$ increases slightly from 18.006% (for a CMG with 2 loads) to 18.879% (for a CMG with 10 loads). Similarly, $\Delta V_{critical}$ increases slightly from 6.680 to 6.802%.

One more study is conducted to investigate the impact of the increase in the number of the loads in the CMG if their total power demand is kept constant and equal to the total demand of the base case. Fig. 9b illustrates $\Delta f_{critical}$ and $\Delta V_{critical}$ for the CMG in these scenarios where the first data in its both subfigures correspond to the CMG base case. From this figure, it can be seen that $\Delta f_{critical}$ increases slightly from 18.006% (for a CMG with 2 loads) to 18.028% (for a CMG with 10 loads) if the total demand of the loads is the same in all scenarios. Likewise, $\Delta V_{critical}$ increases slightly from 6.680 to 6.704%.

To evaluate the impact of the load power factor on the SSS analysis of the CMG system, another study is carried out. Let us assume that the power factor of the load of MG-2 is varied from 0.9 to 0.1 while its total apparent power is kept constant in all scenarios. Fig. 9c illustrates $\Delta f_{critical}$ and $\Delta V_{critical}$ for the CMG in these scenarios. From this figure, it can be seen that $\Delta f_{critical}$ increases slightly from 18.028% (for a load with power factor of 0.9 lagging) to 18.181% (for a load with power factor of 0.1 lagging) if the apparent power of the load is the same in all scenarios. Likewise, $\Delta V_{critical}$ increases slightly from 6.680 to 6.704%.

The above analyses show that a change in the number, demand and power factor of the loads in one of the MGs does not affect the stability margins of the CMG strongly. A similar conclusion can also be made for the stability margins of an MG when the number, demand and power factor of its loads are increased.

4.2.3. Impact of Lines

First, a study is conducted to analyze the SSS of the CMG system with respect to the length of the lines. For this, let us assume that the length of the lines of MG-2 is varied from 0.01 to 10 times of the length of MG-2 base case while the Ω/km impedance of all lines are thought to be the same. Fig. 10a illustrates $\Delta f_{\text{critical}}$ and $\Delta V_{\text{critical}}$ for the CMG in these scenarios. From this figure, it can be seen that $\Delta f_{\text{critical}}$ increases from 11.918% (for 1% of the nominal line length) to 17.417% (for 10 times of the nominal line length). Likewise, $\Delta V_{\text{critical}}$ increases from 4.276% (for 1% of the nominal line length) to 16.539% (for 5 times of the nominal line length), while no instability is observed when the line length is more than 5 times of the nominal line length.

To assess the impact of the line X/R ratio, a new study is carried out. Let us assume that the X/R ratios of the lines of MG-2 are varied from 0.1 to 10. Let us consider the following 6 scenarios of:

- scenario-1: R_{line} = 0.2 Ω, X/R = 0.1
- scenario-2: R_{line} = 0.2 Ω, X/R = 1
- scenario-3: R_{line} = 0.2 Ω, X/R = 10
- scenario-4: X_{line} = 0.2 Ω, X/R = 0.1
- scenario-5: X_{line} = 0.2 Ω, X/R = 1
- scenario-6: X_{line} = 0.2 Ω, X/R = 10

$\Delta f_{\text{critical}}$ and $\Delta V_{\text{critical}}$ of these 6 scenarios are shown in Fig. 10b. From this figure, it can be seen that for the same line resistance, $\Delta f_{\text{critical}}$ increases from 17.875% (for scenario-1 with X/R = 0.1) to 19.185% (for scenario-3 with X/R = 10). However, $\Delta V_{\text{critical}}$ is not affected and is 6.680%. On the other hand, for the same line reactance, $\Delta V_{\text{critical}}$ increases from 4.497% (for scenario-4 with X/R = 0.1) to 6.680% (for scenario-5 with X/R = 1) while no instability is observed for scenario-6 with X/R = 10.

4.2.4. Impact of System Topology

Another study is conducted to evaluate the impact of the MG topology on the stability of the CMG. In the CMG base case, discussed above, both MG-1 and MG-2 are assumed to have a loop configuration. Now, let us assume that MG-2 has a radial configuration (assuming that the connection between bus-3 and bus-4 is broken). The analysis reveals that in such a scenario, the CMG is critically stable for $\Delta f_{\text{critical}}$ = 18.072% and $\Delta V_{\text{critical}}$ = 6.704%. The analysis is repeated for the other lines as well and a negligible difference is observed between the stability margins of the CMG when MG-2 has a loop or radial structure. This is mainly due to the reason that the line states do not have a significant impact on the critical eigenvalues of the system.

4.3. Stability of an MG with BES Systems

Let us assume one or multiple BES systems are to be connected to an MG. The impacts of the number, energy capacity, RoD, and SoC of the BES systems on the stability of the MG are evaluated below:

4.3.1. Impact of Number of BES Systems

To investigate the impact of the number of BES systems on the stability of an MG, the system of MG-1 base case is considered in which the number of the connected BES systems is increased sequentially from 0 to 8. In all scena-

rios, the SoC, RoD and the energy capacity of the BES systems are thought to be the same and equal to the values given in Table A1 in the Appendix. Fig. 11a illustrates $\Delta f_{\text{critical}}$ and $\Delta V_{\text{critical}}$ for MG-1 in these scenarios where the first data in its both subfigures correspond to MG-1 base case. From these figures, it can be seen that $\Delta f_{\text{critical}}$ reduces slightly from 19.010% (for MG-1 base case) to 17.046% (for MG-1 with one BES system). It is further reduced to 12.049% (for MG-1 with 8 BES systems). Similarly, $\Delta V_{\text{critical}}$ reduces slightly from 7.317% (for MG-1 base case) to 6.042% (for MG-1 with one BES system) and reduces to 4.301% (for MG-1 with 8 BES systems).

In the above analysis, it was assumed that the total energy storage capacity of MG-1 increases as more BES systems are connected. To analyze the impact of the increase in the number of the BES systems if their total energy capacity is kept constant, a different study is conducted. In this study, the number of BES systems connected to MG-1 is increased sequentially from 1 to 8 while the total energy capacity is kept constant in all scenarios. The SoC and the RoD of all BES systems are again thought to be the same and equal to those of the previous study. Fig. 11b illustrates $\Delta f_{\text{critical}}$ and $\Delta V_{\text{critical}}$ for MG-1 in these scenarios. This figure illustrates the same variations in the stability margins as the previous study. Thus, it can be seen that the stability margins of MG-1 are not affected by the total energy capacity of its BES systems.

4.3.2. Impact of RoD of BES Systems

A new study is carried out to evaluate the impact of the RoD of the BES systems. Let us consider MG-1 base case in which one BES system is connected. The SoC and energy capacity of the BES is the same as those in Section 4.3.1 while its RoD is assumed to be increased from 40 to 200% of the previous study. Fig. 11c illustrates $\Delta f_{\text{critical}}$ and $\Delta V_{\text{critical}}$ for MG-1 in these scenarios. From this figure, it can be seen that $\Delta f_{\text{critical}}$ increases from 4.062% (for 40% of the nominal RoD) to 19.097% (for 200% of the nominal RoD). Similarly, $\Delta V_{\text{critical}}$ increases from 2.780 to 7.489%.

4.3.3. Impact of SoC of BES Systems

To analyze the impact of the SoC of the BES systems, an additional study is conducted. Let us consider MG-1 base case in which one BES system is connected. The RoD and energy capacity of the BES is the same as those in Section 4.3.1 while its SoC is thought to be decreased from 100 to 20%. Fig. 11d illustrates $\Delta f_{\text{critical}}$ and $\Delta V_{\text{critical}}$ for MG-1 in these scenarios. From this figure, it can be seen that $\Delta f_{\text{critical}}$ decreases from 17.046% (for SoC of 100%) to 7.968% (for SoC of 20%) while $\Delta V_{\text{critical}}$ increases from 6.042 to 6.974%. The decrease in $\Delta f_{\text{critical}}$ is due to lower capability in supplying active power by the BES for smaller SoCs while the increase in $\Delta V_{\text{critical}}$ is due to the fact that a larger portion of the converter of the BES system can be used for reactive power exchange.

This analysis is further extended to consider more BES systems. As an example, $\Delta f_{\text{critical}}$ and $\Delta V_{\text{critical}}$ variation for MG-1 with two BES systems is illustrated in Fig. 11e while the same quantities for MG-1 with three BES systems are as shown in Fig. 11f. From these figures, it can be seen that presence of a BES with a smaller SoC reduces $\Delta f_{\text{critical}}$ of the MG but increases its $\Delta V_{\text{critical}}$. Thus, it is highly beneficial to develop a technique such as those discussed in Section 2.2 which can facilitate equal variation in the SoCs of multiple connected BES systems to an MG. The above analyses illustrate that the SoC and RoD of a BES system, in addition to its VSC and filter system, signifi-

cantly affect the stability margins of the MG while its energy capacity does not affect them.

5. Conclusions

When overloading is observed in the isolated MGs of remote areas, the MG can be supported by local BES systems and by importing power from a neighboring MG, after they are interconnected temporarily. Thus, such MGs will experience a transformation in their structure to reduce the rate and necessity of load-shedding. Any transformation should not lead to instability in the new system; thus, an eigenanalysis-based small signal stability is proposed and developed in this paper and has a decision-making function prior to any transformation.

Through the numerical analyses for two isolated MGs, it is illustrated that the loci of the operating point eigenvalues of the new system, after coupling them, is approximately within the same loci of the operating point eigenvalues of each system, when operating independently. Furthermore, it is seen that the critical eigenvalues of the new system are dominantly influenced by the same effective states of the critical eigenvalues of each system. Two new marginal stability indices were defined to compare the stability of the new system versus each of the MGs numerically. By the help of these indices and after a sensitivity analysis over the droop coefficients, it is revealed that the MG with lower stability margins causes a drop in the stability margins of the other MG after they are coupled. It is also seen that the stability margins of the new system are strongly affected by the nominal power of the DERs and their ratios while no significance variation was observed versus the number, demand and power factor of the loads. In addition, it is observed that the length and X/R ratio of the lines of the MGs can affect the stability of the new system while no impact was observed when one of the MGs had a loop or radial configuration. The analysis also revealed that the stability of the MG closely corresponds to the SoC and RoD of the BES systems while it was not affected by the total energy capacity of the BES systems.

In summary, it is discovered through the studies that the stability of an MG needs to be cautiously checked prior to the connection of a BES system or another neighboring MG, as developing a list of general stability guidelines is not straightforward and fully depends on the conditions of the newly created system.

This study had focused on sustainable MGs of future remote areas, in which all electricity demand is generated by the help of converter-interfaced resources. The study can be expanded to include the presence of inertial sources such as diesel/gas-based generators if they are assumed to share a portion of the load in the MGs. Furthermore, the analysis did not consider a dynamic variation in the ratio of the output power of the DERs or a cost-prioritized droop control, which can be a topic for future research in this area. It is also to be highlighted that this study was focused on the dynamic stability of the CMGs. To guarantee that the system will not fail during the transient process of interconnecting with another MG or connection of a BES system, a transient stability should also be considered and accompanied by the dynamic stability, which can be a topic for future research.

Appendix

The technical parameters of the network under consideration in Fig. 3 are provided in Table A1.

References

[1] M. Roach, “Community power and fleet microgrids: meeting climate goals, enhancing system resilience, and

stimulating local economic development," *IEEE Electrification Magazine*, vol.2, no.1, pp.40-53, 2014.

[2] G. Yuan, "Rural electrification goes local: recent innovations in renewable generation, energy efficiency, and grid modernization," *IEEE Electrification Magazine*, vol.3, no.1, pp.16-24, 2015.

[3] A. Zomers, "Remote access: context, challenges, and obstacles in rural electrification," *IEEE Power and Energy Magazine*, vol.12, no.4, pp.26-34, 2014.

[4] Facts about Remote Australia, Cooperative Research Centre for Remote Economic Participation, 2015. http://crc-rep.com/about-remote-australia

[5] R. Paleta, A. Pina, and C.A.S. Silva, "Polygeneration energy container: Designing and testing energy services for remote developing communities," *IEEE Trans. Sustainable Energy*, vol.5, pp.1348-1355, 2014.

[6] M. Arriaga, C.A Canizares, and M. Kazerani, "Northern lights: access to electricity in Canada's northern and remote communities," *IEEE Power and Energy Magazine*, vol.12, pp.50 - 59, 2014.

[7] Y. Tan, L. Meegahapola, and K.M. Muttaqi, "A review of technical challenges in planning and operation of remote area power supply systems," *Renewable and Sustainable Energy Reviews*, vol.38, pp.876-889, 2014.

[8] Z. Bie, and Y. Lin, "An overview of rural electrification in China: history, technology, and emerging trends," *IEEE Electrification Magazine*, vol.3, no.1, pp.36-47, 2015.

[9] H. Louie, E. O'Grady, V. Van Acker, *et al.*, "Rural off-grid electricity service in sub-Saharan Africa," *IEEE Electrification Magazine*, vol.3, no.1, pp.7-15, 2015.

[10] K.C. Latoufis, T.V. Pazios, and N.D. Hatziargyriou, "Locally manufactured small wind turbines: empowering communities for sustainable rural electrification," *IEEE Electrification Magazine*, vol.3, no.1, pp.68-78, 2015.

[11] N. Mendis, K.M. Muttaqi, S. Perera, and M.N. Uddin, "Remote area power supply system: an integrated control approach based on active power balance," *IEEE Industry Applications Magazine*, vol.21, no.2, pp.63-76, 2015.

[12] T. Kerdphol, K. Fuji, Y. Mitani, *et al.*, "Optimization of a battery energy storage system using particle swarm optimization for stand-alone microgrids," *International Journal of Electrical Power & Energy Systems*, vol.81, pp.32-39, 2016.

[13] K. Ubilla, G.A. Jimenez-Estevez, R. Hernadez, R., *et al.* "Smart microgrids as a solution for rural electrification: ensuring long-term sustainability through cadastre and business models" *IEEE Trans. Sustainable Energy*, vol.5, pp.1310-1318, 2014.

[14] J. Clavier, F. Bouffard, D. Rimorov, and G. Joós, "Generation dispatch techniques for remote communities with flexible demand," *IEEE Trans. Sustainable Energy*, vol.6, no.3, pp.720-728, 2015.

[15] E. Hajipour, M. Bozorg, and M. Fotuhi-Firuzabad, "Stochastic capacity expansion planning of remote microgrids with wind farms and energy storage," *IEEE Trans. Sustainable Energy*, vol.6, no.2, pp.491-498, 2015.

[16] P. Meneses de Quevedo, J. Allahdadian, J. Contreras, and G. Chicco, "Islanding in distribution systems considering wind power and storage," *Sustainable Energy, Grids and Networks*, vol.5, pp.156-166, 2016.

[17] P. Pinceti, M. Vanti, C. Brocca, *et al.*, "Design criteria for a power management system for microgrids with renewable sources," *Electric Power Systems Research*, vol.122, pp.168-179, 2015.

[18] Y.A.I. Mohamed, and T.H.M. El-Fouly, "Supply-adequacy-based optimal construction of microgrids in smart distribution systems," *IEEE Trans. on Smart Grid*, vol.3, no.3, pp.1491-1502, 2012.

[19] Urban Rudez, Rafael Mihalic, "Predictive underfrequency load shedding scheme for islanded power systems with renewable generation," *Electric Power Systems Research*, vol.126, pp.21-28, 2015.

[20] C. Brivio, S. Mandelli, and M. Merlo, "Battery energy storage system for primary control reserve and energy arbitrage," *Sustainable Energy, Grids and Networks*, vol.6, pp.152-165, 2016.

[21] R.H. Lasseter, "Smart distribution: coupled microgrids," *Proceedings of the IEEE*, vol.99, no.6, pp.1074-1082, 2011.

[22] Z. Wang, and J. Wang, "Self-healing resilient distribution systems based on sectionalization into microgrids," *IEEE Trans. Power Systems*, vol.30, no.6, pp.3139-3149, 2015.

[23] Z. Wang, B. Chen, J. Wang, and C. Chen, "Networked microgrids for self-healing power systems," *IEEE Trans. Smart Grid*, doi:10.1109/TSG.2015.2427513.

[24] H. Dagdougui, A. Ouammi, and R. Sacile, "Optimal control of a network of power microgrids using the pontryagin's minimum principle," *IEEE Trans. Control System Technology*, vol.22, no.5, pp.1942-1948, 2014.

[25] Y. Zhang, L. Xie, and Q. Ding, "Interactive control of coupled microgrids for guaranteed system-wide small signal stability," *IEEE Trans. Smart Grid*, doi:10.1109/TSG.2015.2495233.

[26] F. Shahnia, R.P.S. Chandrasena, S. Rajakaruna, and A. Ghosh, "Primary control level of parallel distributed energy resources converters in system of multiple interconnected autonomous microgrids within self-healing networks," *IET Generation, Transmission & Distribution*, vol.8, pp.203-222, 2014.

[27] Y. Zhang, and L. Xie, "Online dynamic security assessment of microgrid interconnections in smart distribution systems," *IEEE Trans. Power Syst.*, vol.30, no.6, pp.3246-3254, 2015.

[28] I.P. Nikolakakos, H.H. Zeineldin, M.S. El-Moursi, and N.D. Hatziargyriou, "Stability evaluation of interconnected multi-inverter microgrids through critical clusters," *IEEE Trans. Pow. Sys.*, doi:10.1109/TPWRS.2015.2476826.

[29] I.U. Nutkani, P.C. Loh, and F. Blaabjerg, "Distributed operation of interlinked ac microgrids with dynamic active and reactive power tuning," *IEEE Trans. Industry Applications*, vol.49, no.5, pp.2188-2196, 2013.

[30] E. Pashajavid, F. Shahnia, and A. Ghosh, "Development of a self-healing strategy to enhance the overloading resilience of islanded microgrids," *IEEE Trans. Smart Grid*, doi:10.1109/TSG.2015.2477601.

[31] F. Shahnia, S. Bourbour, and A. Ghosh, "Coupling neighboring microgrids for overload management based on dynamic multicriteria decision-making," *IEEE Trans. Smart Grid*, doi:10.1109/TSG.2015.2477845.

[32] E. Pashajavid, F. Shahnia, and A. Ghosh, "Overload management of autonomous microgrids,"11th IEEE Int. Conf. on Power Electronics and Drive Systems (PEDS), pp.73-78, Sydney, Australia, June 2015.

[33] R. Majumder, "Some Aspects of Stability in Microgrids," *IEEE Trans. Power Systems*, vol.28, no.3, pp.3243-3252, Aug. 2013.

[34] E.A.A. Coelho, P.C. Cortizo, and P.F.D. Garcia, "Small-signal stability for parallel-connected inverters in stand-alone ac supply systems," *IEEE Trans. Industry Applications*, vol.38, no.2, pp.533-542, 2002.

[35] A. Haddadi, B. Boulet, A. Yazdani, and G. Joos, "A μ-based approach to small-signal stability analysis of an interconnected distributed energy resource unit and load," *IEEE Trans. Power Delivery*, vol.30, no.4, pp.1715-1726, 2015.

[36] J. Sun, "Small-signal methods for ac distributed power systems–a review," *IEEE Trans. Power Electronics*, vol.24, no.11, pp.2545-2554, 2009.

[37] N. Pogaku, M. Prodanovic, and T.C. Green, "Modeling, analysis and testing of autonomous operation of an inverter-based microgrid," *IEEE Trans. Power Electronics*, vol.22, no.2, pp.613-625, 2007.

[38] M.N. Marwali, J.W. Jung, and A. Keyhani, "Stability analysis of load sharing control for distributed generation systems," *IEEE Trans. Energy Conversion*, vol.22, no.3, pp.737-745, 2007.

[39] D.K. Dheer, N. Soni, and S. Doolla, "Improvement of small signal stability margin and transient response in inverter-dominated microgrids," *Sustainable Energy, Grids and Networks*, vol.5, pp.135-147, 2016.

[40] Y.A.R.I. Mohamed, and E.F. El-Saadany, "Adaptive decentralized droop controller to preserve power sharing stability of paralleled inverters in distributed generation microgrids," *IEEE Trans. Power Electronics*, vol.23, no.6, pp.2806-2816, 2008.

[41] R. Majumder, B. Chaudhuri, A. Ghosh, *et al.*, "Improvement of stability and load sharing in an autonomous microgrid using supplementary droop control loop," *IEEE Trans. Power Systems*, vol.25, no.2, pp.796-808, 2010.

[42] M. Rasheduzzaman, J.A. Mueller, and J.W. Kimball, "An accurate small-signal model of inverter- dominated islanded microgrids using dq reference frame," *IEEE Journal of Emerging and Selected Topics in Power Electronics*, vol.2, no.4, pp.1070-1080, 2014.

[43] E. Pashajavid, F. Shahnia, and A. Ghosh, "Interconnection of two neighboring autonomous microgrids based on small signal analysis," 9th Int. Conf. on Power Electronics (ICPE-ECCE Asia), pp.213-220, 2015.

[44] F. Katiraei, M.R. Iravani, and P.W. Lehn, "Small-signal dynamic model of a micro-grid including conventional and electronically interfaced distributed resources," *IET Generation, Transmission & Distribution*, vol.1, no.3, pp.369-378, 2007.

[45] Y. Guan, J.C. Vasquez, J.M. Guerrero, *et al.*, "Frequency stability of hierarchically controlled hybrid photovoltaic-battery-hydropower microgrids," *IEEE Trans. Industry Applications*, vol.51, no.6, pp.4729-4742, 2015.

[46] B.M. Eid, N.A. Rahim, J. Selvaraj, and A.H. El-Khateb, "Control methods and objectives for electronically coupled distributed energy resources in microgrids," *IEEE Systems Journal*, doi:10.1109/JSYST.2013.2296075.

[47] K.O. Oureilidis, and C.S. Demoulias, "A decentralized impedance-based adaptive droop method for power loss reduction in a converter-dominated islanded microgrid," *Sustainable Energy, Grids and Networks*, vol.5, pp.39-49, 2016.

[48] I.U. Nutkani, P.C. Loh, P. Wang, and F. Blaabjerg, "Cost-prioritized droop schemes for autonomous ac microgrids," *IEEE Trans. Power Elect.*, vol.30, no.2, pp.1109-1119, 2015.

[49] T. Hosseinimehr, F. Shahnia, and A. Ghosh, "Power sharing control of batteries within autonomous microgrids based on their state of charge," 25th Australasian Universities Power Engineering Conference (AUPEC), pp.1-5,

Wollongong, Australia, 2015.

[50] Y.S. Kim, E.S. Kim, and S.I. Moon, "Frequency and voltage control strategy of standalone microgrids with high penetration of intermittent renewable generation systems," *IEEE Trans. in Power Systems*, doi:10.1109/TPWRS.2015.2407392.

[51] P. Kundur, *Power System Stability and Control*, McGraw-Hill, 1994.

[52] W.A. Hashlamoun, M.A. Hassouneh, and E.H. Abed, "New results on modal participation factors: revealing a previously unknown dichotomy," *IEEE Trans. Automatic Control*, vol.54, no.7, pp.1439-1449, 2009.

[53] A. Jamehbozorg, and G. Radman, "Small signal analysis of power systems with wind and energy storage units," *IEEE Trans. Power Systems*, vol.30, no.1, pp.298-305, 2015.

Table 1. Characteristics of the critical eigenvalues of MG-1, MG-2 and CMG base cases.

Eigenvalues		σ [1/s]	υ [rad/s]	ζ [%]	ω_n [rad/s]	T [s]	$NoC_{50\%}$	Affecting
MG-1 Base Case	λ_1 - λ_2	– 7.807	± 309.840	2.52	309.938	0.0203	4.378	*m*, *n*
MG-2 Base Case	λ_1 - λ_2	– 13.351	± 309.819	4.31	310.107	0.0203	2.560	*m*, *n*
	λ_3 - λ_4	– 6.969	± 309.819	2.25	309.898	0.0203	4.904	*m*, *n*
	λ_5 - λ_6	– 10.191	± 309.819	3.29	309.987	0.0203	3.353	*m*, *n*
	λ_7 - λ_8	– 314.159	± 314.159	70.71	444.288	0.0200	0.110	*m*
CMG Base Case	λ_1 - λ_2	–17.147	±309.837	5.52	310.311	0.0202	1.993	*m*, *n*
	λ_3 - λ_4	–9.336	±309.826	3.01	309.966	0.0202	3.660	*m*, *n*
	λ_5 - λ_6	–6.807	±309.825	2.19	309.899	0.0202	5.020	*m*, *n*
	λ_7 - λ_8	–7.799	±309.826	2.51	309.924	0.0202	4.382	*m*, *n*
	λ_9 - λ_{10}	–314.159	±314.159	70.71	444.288	0.0200	0.110	*m*, *n*
	λ_{11} - λ_{12}	–15.482	±45.165	32.42	47.745	0.1391	0.321	*m*

Table. A1. Parameters of the network under consideration in Fig. 3.

MG-1 and MG-2 parameters: 3-phase, 4-wire, multiple earthed neutral (MEN) type
V_{base} = 230 V, V^{max} = 241.5 V, V^{min} = 218.50 V,
$f_{nominal}$ = 50 Hz, f^{max} = 50.5 Hz, f^{min} = 49.5 Hz,
Z_{load} = 50.57 + j 16.6504 Ω/phase
Z_{line} = 0.1 + j 0.1 Ω/phase, $Z_{tie\text{-}line}$ = 0.1 + j 0.1 Ω/phase
DER parameters: P_{DER}^{cap} = 3 kW, S_{DER}^{cap} = 3.9 kVA, L_T = 13.6 mH
BES system parameters: E_{BES}^{cap} = 5 kWhr, RoD_{BES}^{cap} = 2 kW, S_{BES}^{cap} = 2.6 kVA
VSC Structure: L_f = 0.37 mH, C_f = 50 μF

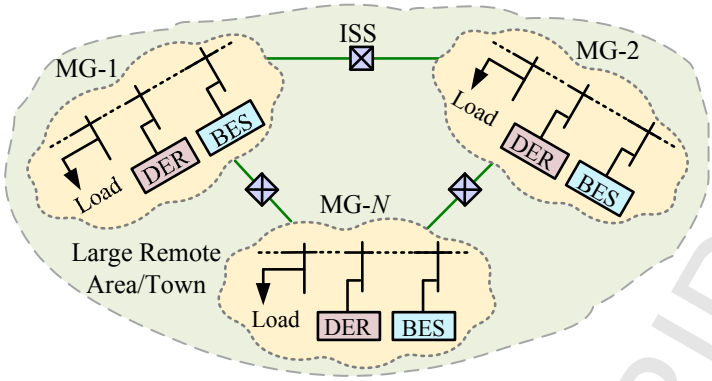

Fig. 1. Sample illustration of a large remote town supplied by 3 isolated MGs.

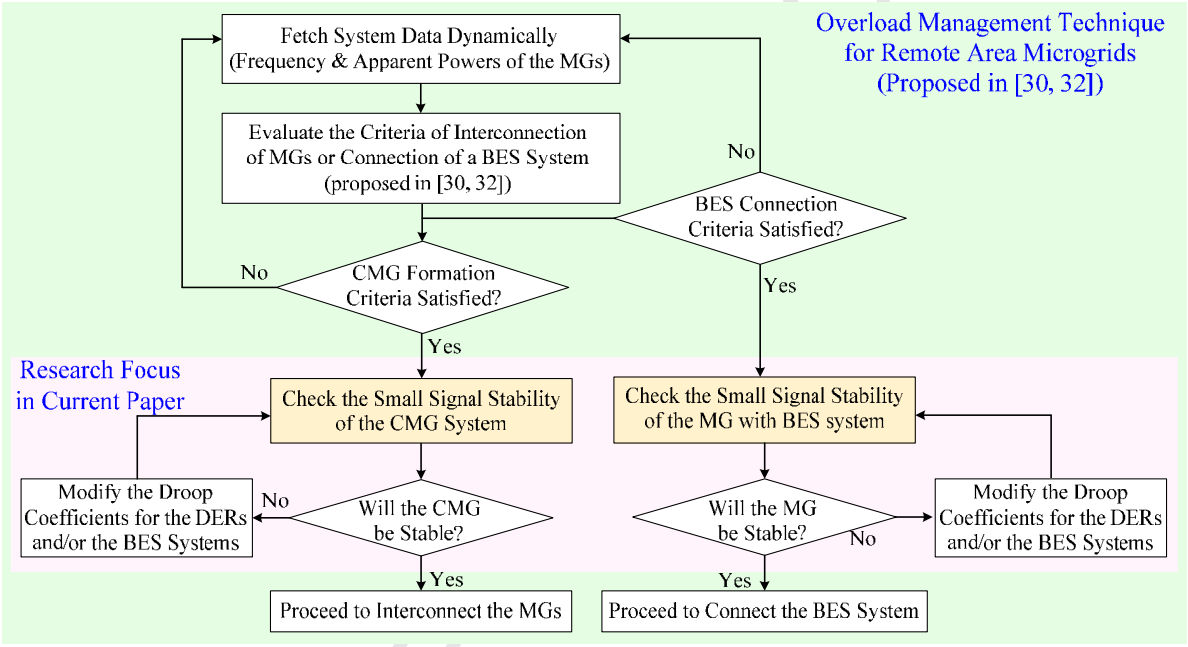

Fig. 2. Operation flowchart for the overload management technique of remote area MGs and the main research scope of this paper.

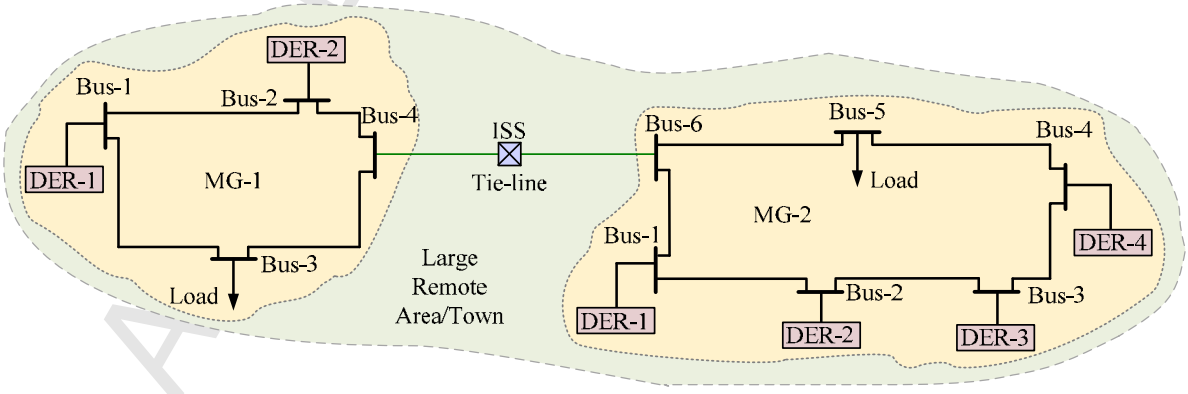

Fig. 3. Considered remote area network for numerical analyses.

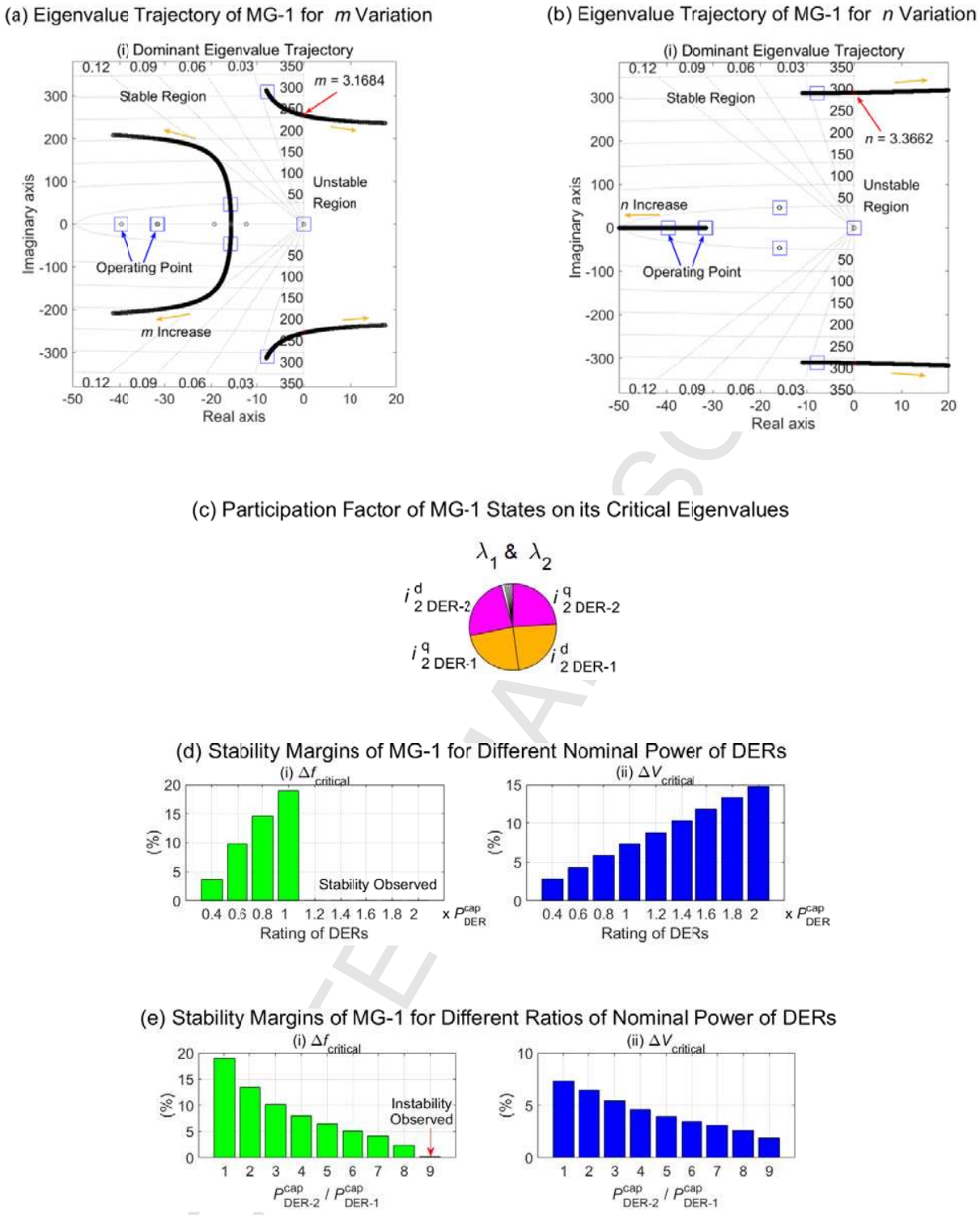

Fig. 4. (a) Eigenvalue trajectory of MG-1 for m variation, (b) Eigenvalue trajectory of MG-1 for n variation, (c) Participation factors of MG-1 effective states on its dominant eigenvalues, (d) Stability margins of MG-1 for DERs with different nominal powers, (e) Stability margins of MG-1 for DERs with different ratios of nominal powers.

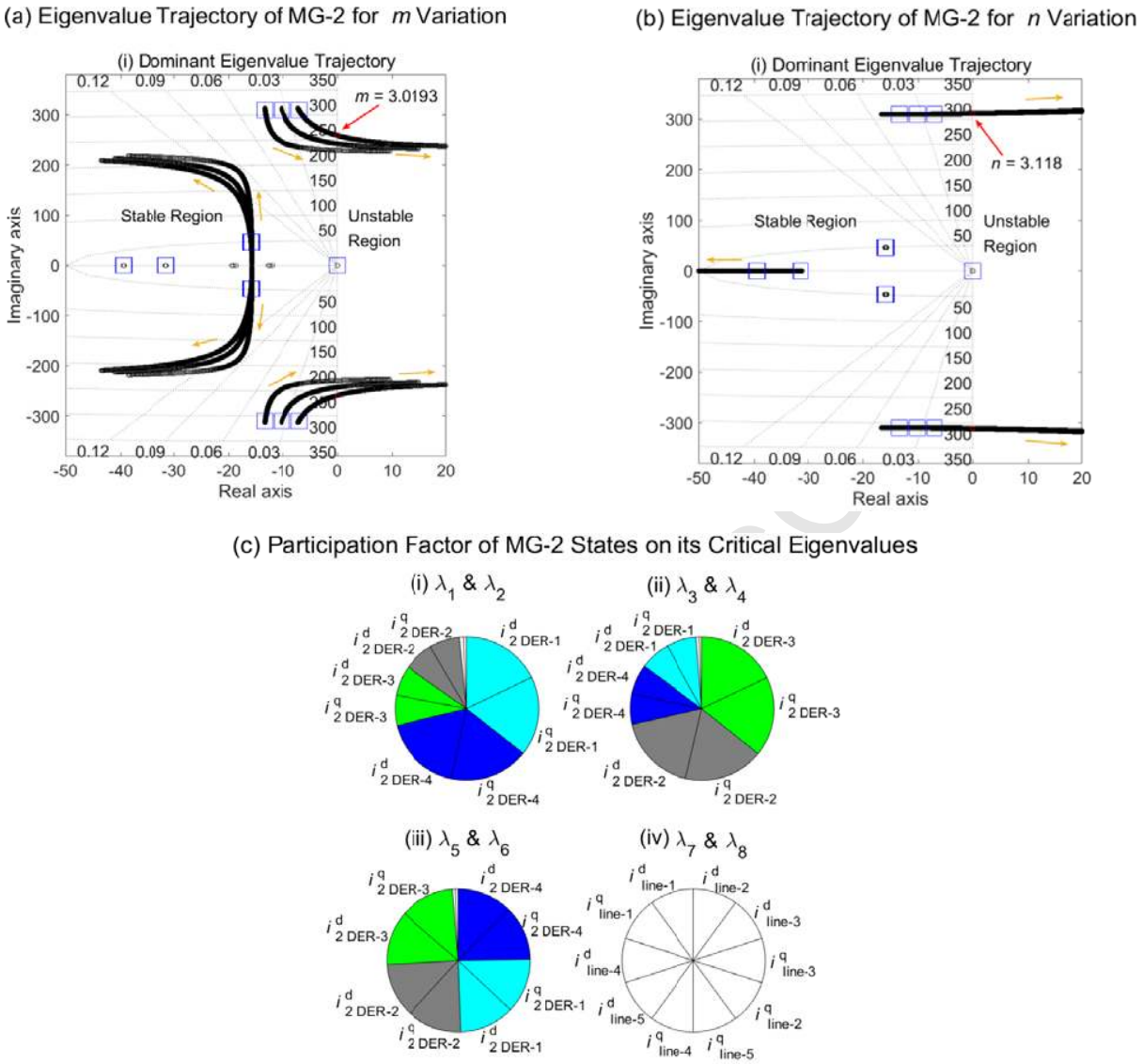

Fig. 5. Eigenvalue trajectory of MG-2 for (a) *m* variation, (b) *n* variation, (c) Participation factors of of MG-2 effective states on its dominant eigenvalues.

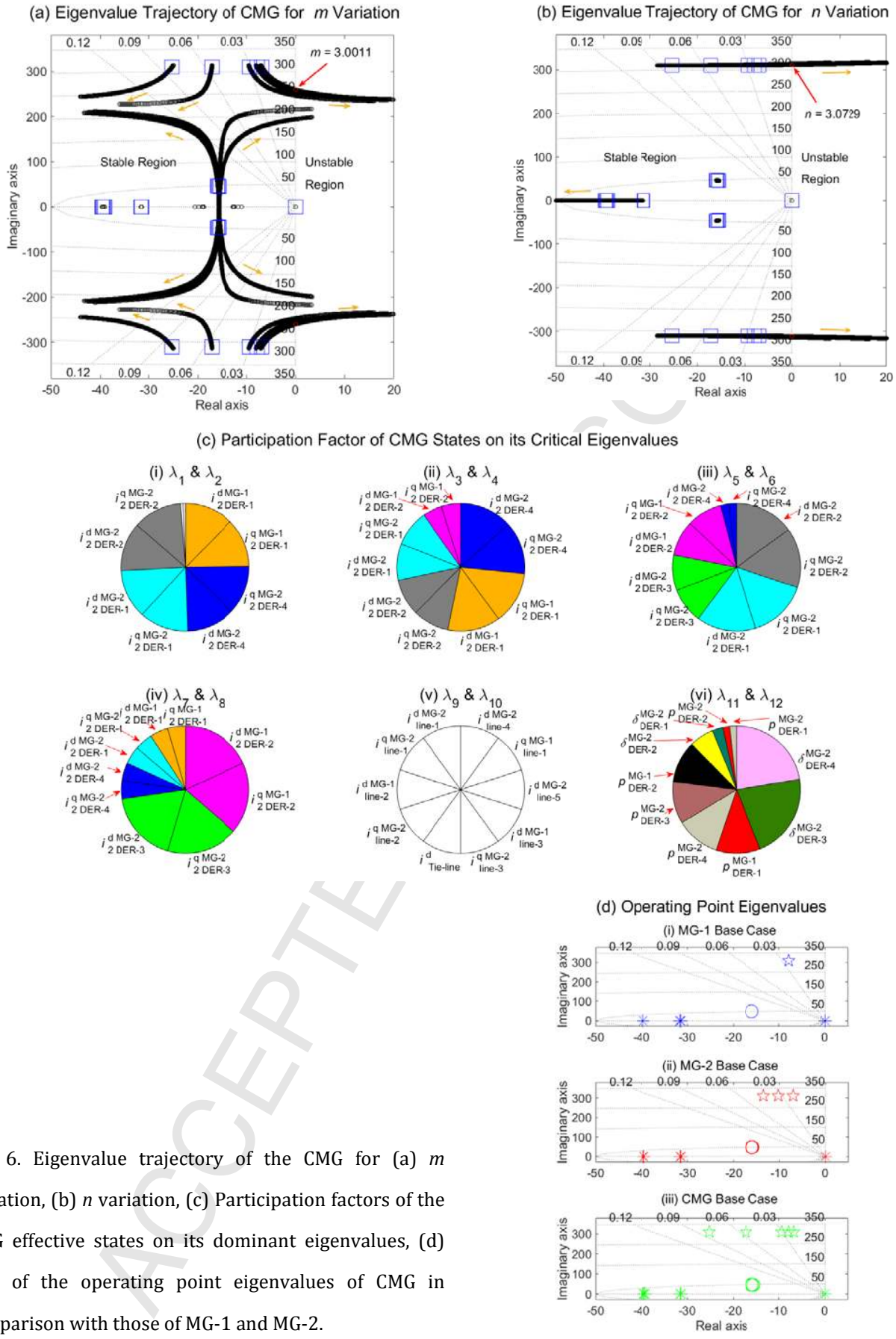

Fig. 6. Eigenvalue trajectory of the CMG for (a) *m* variation, (b) *n* variation, (c) Participation factors of the CMG effective states on its dominant eigenvalues, (d) Loci of the operating point eigenvalues of CMG in comparison with those of MG-1 and MG-2.

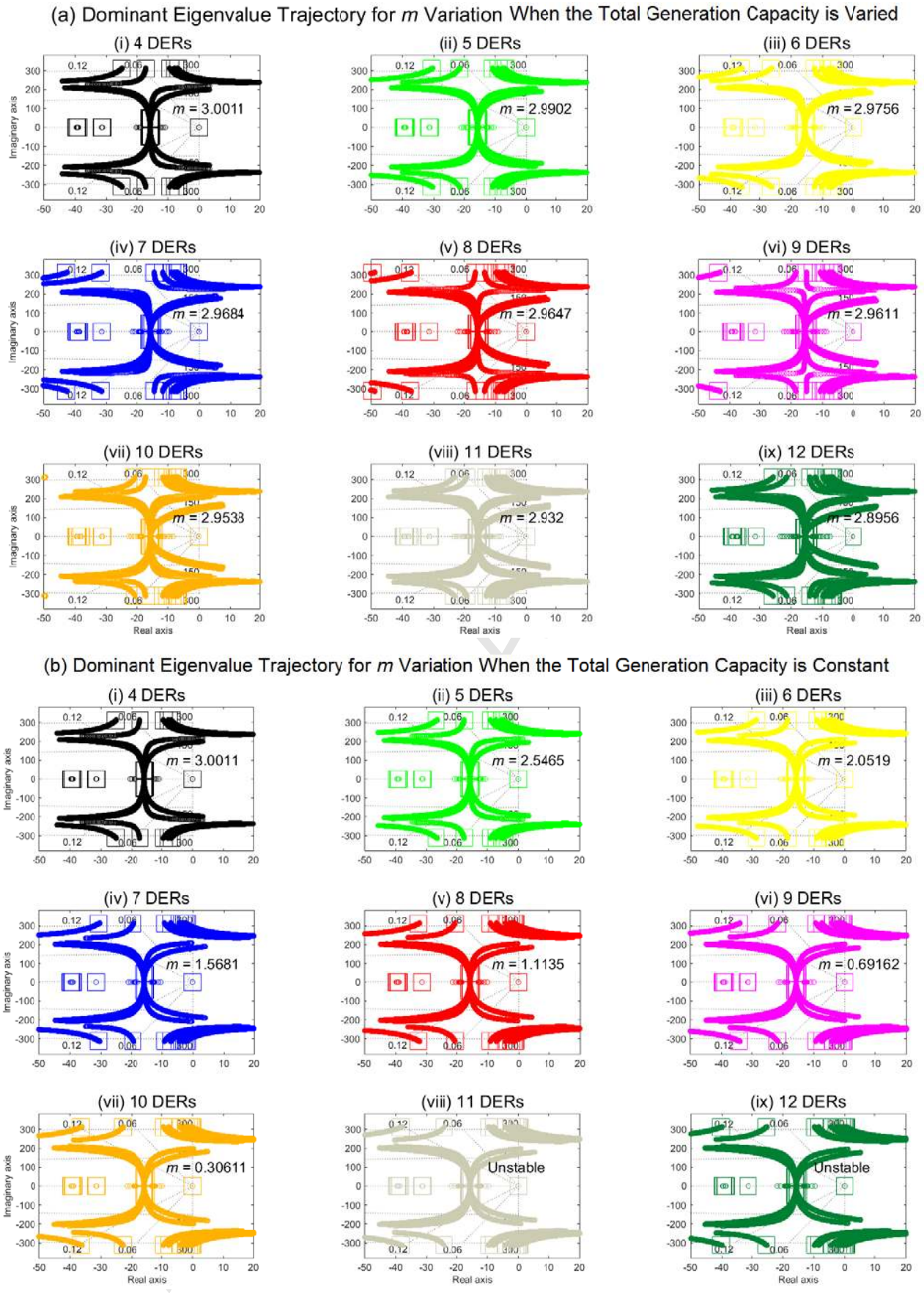

Fig. 7. Evolution of the dominant eigenvalue trajectory for the CMG versus an increase in the number of the DERs of MG-2 for *m* variation, assuming the total generation capacity in MG-2 is: (a) increasing, (b) constant.

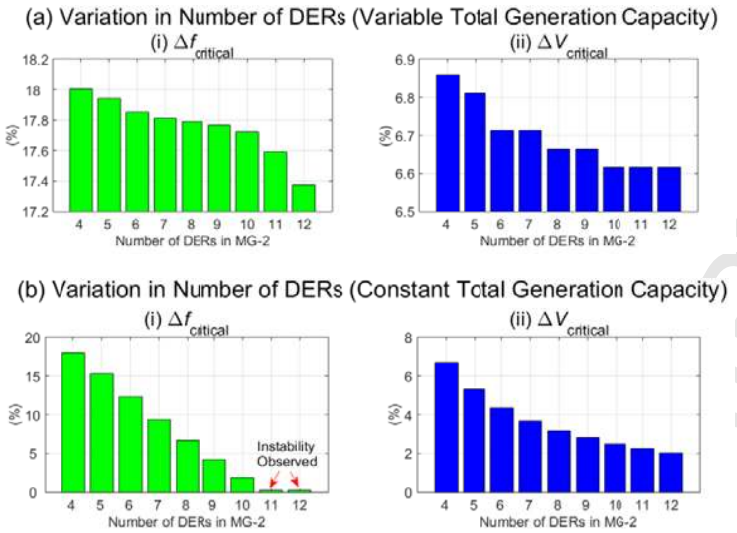

Fig. 8. Stability margins of the CMG for an increase in the number of DERs of MG-2 assuming that the total generation capacity of MG-2 is: (a) increased, (b) constant.

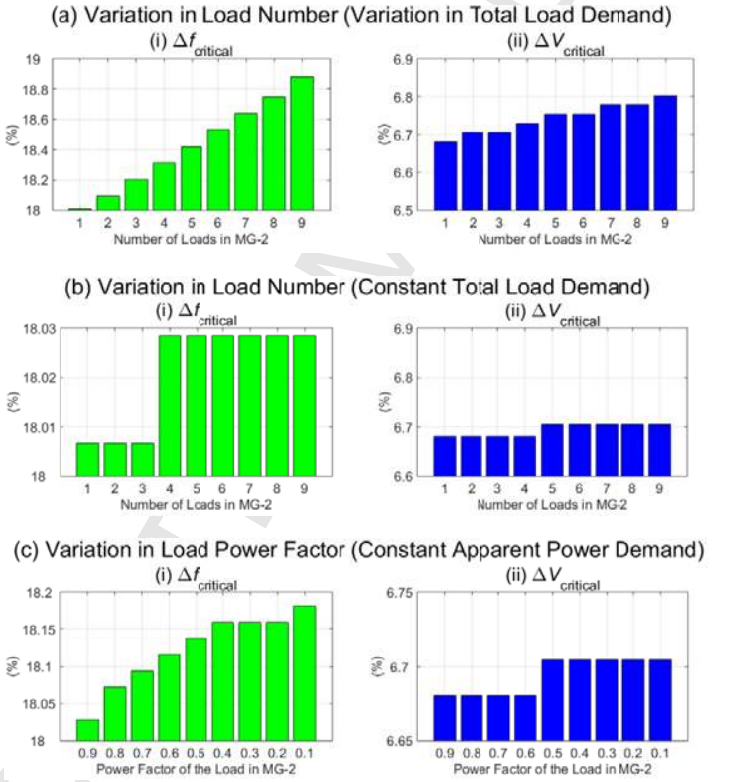

Fig. 9. Variation in the stability margins of the CMG versus the loads of MG-2: (a) for an increase in the number of loads, assuming that the total load demand is increased, (b) for an increase in the number of loads, assuming that the total load demand is constant, (c) for a decrease in the power factor of the load, assuming that the load apparent power is constant.

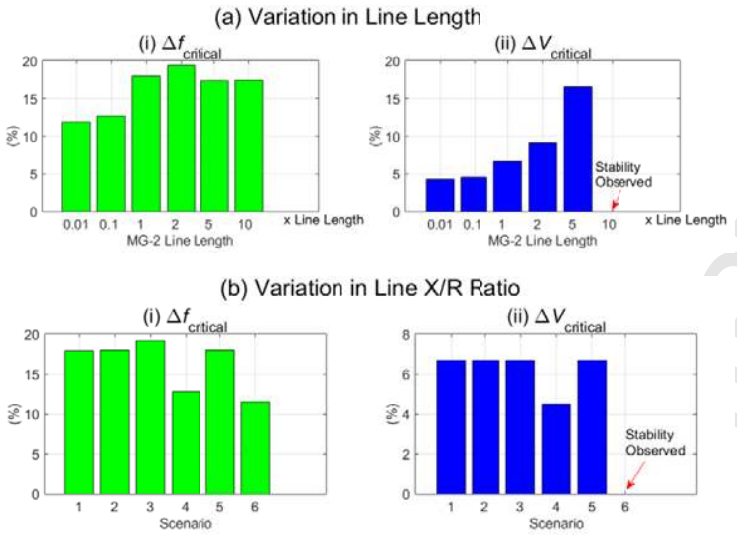

Fig. 10. Variation in the stability margins of the CMG versus the lines of MG-2: (a) for an increase in the length of the lines, (b) for different X/R ratios of the lines.

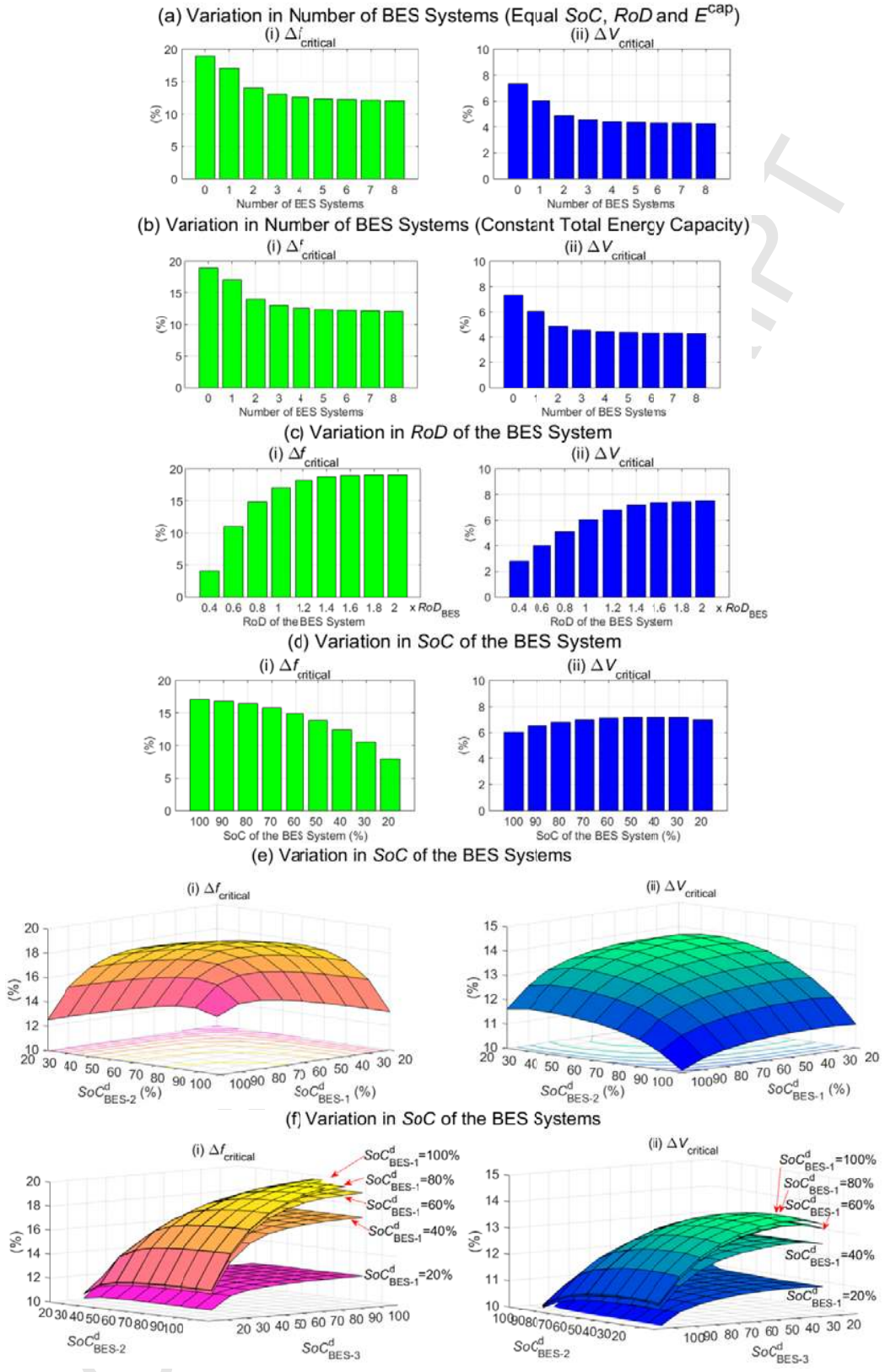

Fig. 11. Variation in the stability margins of MG-1 versus: (a) an increase in the number of BES systems assuming the total energy capacity of MG-1 increases, (b) an increase in the number of BES systems assuming the total energy capacity of MG-1 is constant, (c) an increase in the RoD of the BES system, assuming that the SoC of the BES system is 100%, (d) a decrease in the SoC of the BES system, assuming that the RoD of the BES system is 100%, (e) different values of SoCs of the BES systems, for a system with two BES systems, (f) different values of SoCs of the